Journal of Power Sources 186 (2009) 128–132

Contents lists available at ScienceDirect

Journal of Power Sources

journal homepage: www.elsevier.com/locate/jpowsour

Short communication

Behavior of 3 mol% yttria-stabilized tetragonal zirconia polycrystal film prepared by slurry spin coating

Kongfa Chen [a], Yanting Tian [a], Zhe Lü [a,*], Na Ai [a], Xiqiang Huang [a], Wenhui Su [a,b,c]

[a] Center for Condensed Matter Science and Technology, Harbin Institute of Technology, Harbin 150001, China
[b] Department of Condensed Matter Physics, Jilin University, Changchun 130022, China
[c] International Center for Material Physics, Academia, Shenyang 110015, China

ARTICLE INFO

Article history:
Received 23 July 2008
Received in revised form
16 September 2008
Accepted 19 September 2008
Available online 26 September 2008

Keywords:
3YSZ
Electrolyte film
Slurry spin coating
SOFC

ABSTRACT

A dense and uniform 3 mol% yttria-stabilized tetragonal zirconia polycrystal (3YSZ) electrolyte film of 6 μm in thickness was fabricated by slurry spin coating on a porous NiO/3YSZ anode substrate. Composite cathodes of $La_{0.7}Sr_{0.3}MnO_3$ impregnated with $Sm_{0.2}Ce_{0.8}O_{1.9}$ were fabricated on the 3YSZ films. A single cell produced in this way was tested at 700, 750 and 800 °C with hydrogen as fuel and stationary air as oxidant. Test results revealed an open-circuit voltage of 1.04 V at 800 °C, and maximum power density of 551, 895 and 1143 mW cm^{-2} at 700, 750 and 800 °C, respectively. Impedance spectra results demonstrated that the cell performance was determined by the polarization resistance of the cathode.

1. Introduction

Solid oxide fuel cells (SOFCs) have attracted much attention in recent years for their efficient energy conversion, environmental friendliness and high fuel flexibility [1,2]. A recent trend in SOFC research is to keep the operating temperature below 800 °C to slow down the degradation of cell components, improve the cell design flexibility, and decrease the manufacturing costs [3]. However, a decrease in operational temperature leads to a rapid increase in ohmic resistance across the solid electrolyte, which can be solved by decreasing the thickness of the electrolyte.

A number of fabrication techniques can be used to prepare electrolyte thin films, including sol–gel processing [4,5], tape casting [6,7], screen printing [8] and dip coating [9]. Conventional sol–gel processing requires strict heating and cooling rates, and coating has to be repeated several times, which is complex and time-consuming. Slurry spin coating, a new, simple and inexpensive method for thin-film fabrication, has been successfully developed for the preparation of solid electrolyte films for small cells and stacks [10–12]. Wang et al. [13] used slurry spin coating to fabricate gas-tight anode-supported yttria-stabilized zirconia (YSZ) films for SOFCs and obtained an open-circuit voltage (OCV) as high as 1.06 V and maximum power density of 2005 mW cm^{-2} at 800 °C when hydrogen was used as fuel and ambient air as oxidant.

YSZ is still widely used in SOFCs because of its adequate oxygen ionic conductivity, high ion transport number, good mechanical strength and excellent chemical stability in both oxidizing and reducing environments. The mechanical strength of 3 mol% yttria-stabilized tetragonal zirconia polycrystal (3YSZ) is higher than that of 8 mol% YSZ (8YSZ). Lu et al. [14] added 3YSZ to an 8YSZ electrolyte and observed a remarkable increase in electrolyte strength and an improvement in its fracture toughness, but its electrical conductivity was slightly lower. 3YSZ, an engineering ceramic that is much more cost-effective than 8YSZ, has been widely used for fabrication of SOFCs [15–18]. Therefore, we chose 3YSZ as the electrolyte for fabrication of thin films by slurry spin coating, and investigated the sintering behavior of 3YSZ powders and the electrochemical performance of single cells. Test results revealed that an anode-supported cell with 3YSZ thin film exhibited desirable output performance at an intermediate temperature.

2. Experimental

2.1. Sample preparation and characterization

Nickel oxide (NiO) was synthesized using a precipitation method [19]. 3YSZ (Tosoh, Japan), NiO and wheat flour (used as a pore for-

* Corresponding author. Tel.: +86 451 86418420; fax: +86 451 86418420.
E-mail addresses: kongfachen@163.com (K. Chen), yanting_005@163.com (Y. Tian), lvzhe@hit.edu.cn (Z. Lü).

0378-7753/$ – see front matter © 2008 Elsevier B.V. All rights reserved.
doi:10.1016/j.jpowsour.2008.09.061

mer) were mixed at a weight ratio of 2:2:1 and ground with a pestle in an agate mortar for 2 h to form the primary anode powder. The 3YSZ electrolyte was ball-milled in ethanol for 25 h to decrease the average particle size.

The anode powder and 3YSZ electrolyte particles were pressed into pellets of 6 mm in diameter and 4 mm in height for measurement of sintering shrinkage. A dilatometer (Netzsch DIL 402C/3/G) was used to measure the sintering shrinkage behavior with purge air at 50 ml min^{-1}. Measurements were taken at a heating rate of 5 K min^{-1} in the temperature range 50–1400 °C.

2.2. Fabrication of single cells

The mixed anode powder was compacted into a disc under uniaxial pressure at 200 MPa and the disc was then pre-sintered at 1000 °C for 2 h.

An electrolyte slurry was prepared by blending ball-milled 3YSZ powder with an organic vehicle of ethyl cellulose (chemical reagent grade) and terpineol (analytical reagent grade; 4.5:95.5, w/w) at a 3YSZ/vehicle weight ratio of 30:70. Thin films were fabricated by slurry spin coating three times at a spinning speed of 6 krpm [10]. Each coating layer was heated at 420 °C for 10 min to burn off the organic compounds, followed by sintering at 1400 °C for 4 h.

$La_{0.7}Sr_{0.3}MnO_3/Sm_{0.2}Ce_{0.8}O_{1.9}$ (LSM/SDC) composite cathodes were fabricated using an ion-impregnation process. Ethyl cellulose and terpineol (7:93, w/w) was mixed with LSM prepared via the sol–gel route at a weight ratio of 30:70 to form the cathode slurry, which was then coated onto the 3YSZ films and sintered at 1100 °C for 2 h. After impregnation with $Sm_{0.2}Ce_{0.8}(NO_3)_x$ solution, the composite cathodes were calcined at 850 °C for 1 h.

2.3. Electrochemical performance and microstructure characterization

Single cells were tested using the four-probe method at 700, 750 and 800 °C. Silver paste (DAD-87, Shanghai Research Institute of Synthetic Resin, China) was painted onto the electrode surface as the current collector. The OCV and current–voltage (*I–V*) characteristics were measured using a Solartron SI 1287 electrochemical interface. Impedance measurements were made using a Solartron SI 1260 impedance analyzer combined with the SI 1287 interface in the frequency range 91 kHz–0.1 Hz at an ac voltage of 10 mV. The cell was reduced with humidified hydrogen (H_2, 3 vol.% H_2O) at a flow rate of 100 ml min^{-1}, using stationary air as oxidant. Impedance spectra of the cell were conducted at different hydrogen partial pressures by introducing nitrogen to the anode and at different oxygen partial pressures by introducing oxygen flow to the cathode. Impedance spectra were also conducted at different cell voltages.

The microstructure of single cells was investigated using a scanning electron microscope (SEM, Hitachi S-570).

3. Results and discussion

As shown in Fig. 1a and b, sintering of 3YSZ pellets exhibited a shrinkage peak at 1240 °C, with total sintering shrinkage of 23%. The three peaks for the NiO/3YSZ anode at 105, 245 and 300 °C were due to the volatilization of water, decomposition of pore former, and a decrease in pores made by the pore former, respectively. These processes were complete at 440 °C. Samples then exhibited typical thermal expansion behavior between 440 and 835 °C. The peaks at 500 and 750 °C were caused by noise in the testing environment.

Since the anode substrate was pre-sintered at 1000 °C for 2 h before the electrolyte film was fabricated, sintering changes in the substrate did not occur before 1000 °C. The peaks at 1160 and 1215 °C for the anode substrate were due to shrinkage of NiO and

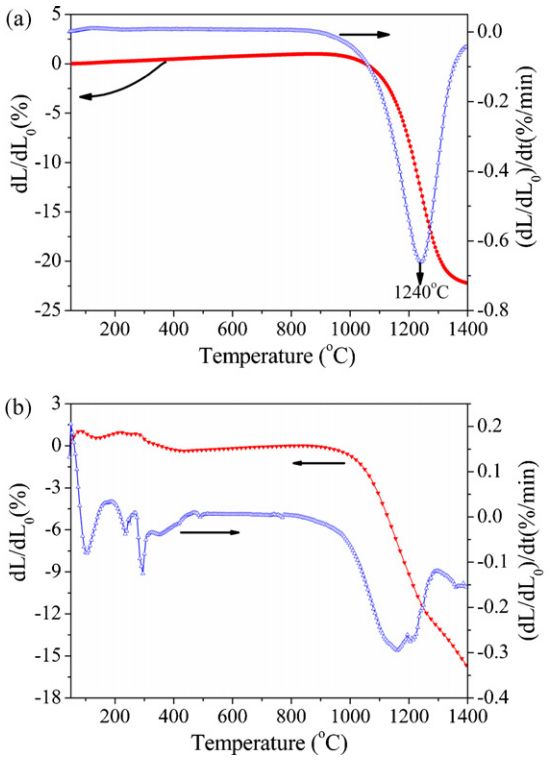

Fig. 1. Sintering behavior and shrinkage rate of (a) 3YSZ and (b) the NiO/3YSZ anode.

3YSZ, respectively. It should be noted that the peak at 1215 °C is slightly lower than that for pure 3YSZ because of the interaction of sintering shrinkage between NiO and 3YSZ. The last shrinkage peak at 1160 °C was due to a decrease in pores, which is disadvantageous for gas transport. Shrinkage of the anode substrate between 1000 and 1400 °C amounted to 15%. If the sintering behavior of the anode substrate does not match that of the film, the cell will bend toward the material that has the higher shrinkage. For example, the cell bends toward the YSZ film when the shrinkage of the thin YSZ layer of approximately 10 μm in thickness exceeds that of the thick anode substrate of approximately 500 μm in thickness [20,21]. Such shrinkage mismatch tends to cause warpage of the bilayer or crack development in the film, which significantly affects subsequent processing, incorporation into stacks and the electrochemical performance of the cell. Various methods have been used to adjust the sintering shrinkage of anodes, such as using different pre-sintering temperatures [21], changing the compaction pressure [22] and using composite pore formers [23]. Song et al. [6] sintered an anode-supported film under pressurized conditions by placing a ceramic plate on top of the bilayer to avoid warpage, an approach that was also used in the present study.

As shown in Fig. 2a, the electrolyte film was very dense, although it has a few shallow pinholes in each of the three film layers, which would be totally occluded by another layer. It is very rare to have a through hole in the electrolyte film. As shown in Fig. 2b, the dense 3YSZ electrolyte film was approximately 6 μm thick and adhered well to the porous anode substrate, indicating a good match between the film and the substrate. The large pores in the anode substrate are caused by burnout of the pore former, which facilitates rapid gas transport. Nanopores produced by the reduction of nickel oxide to nickel can increase both the gas-transport path and the three-phase boundary (TPB) for reaction.

As shown in Fig. 3, the OCV was 1.04 V at 800 °C and remained stable at this value during the whole testing process. This indicates that the 3YSZ film prepared using slurry spin coating was

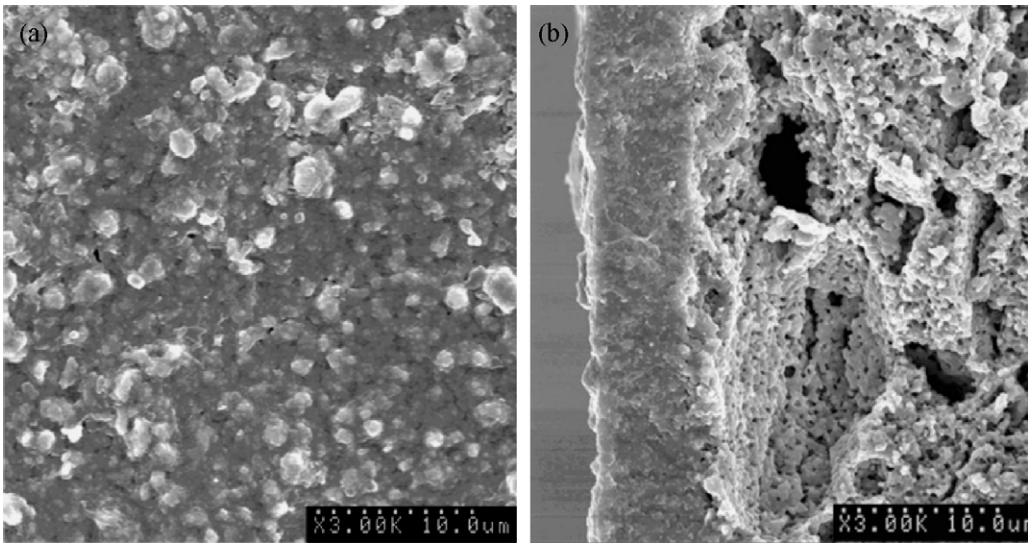

Fig. 2. (a) Surface of the electrolyte film. (b) Cross-section of the single cell.

dense enough and that the reduction of NiO in the anode did not destroy the film. With hydrogen as fuel and ambient air as oxidant, the maximum power density of a single cell was 551, 895 and 1143 mW cm^{-2} at 700, 750 and 800 °C, respectively. The *I–V* curves show negative curvature at high current density, which is associated with concentration polarization of the electrodes. Since the 500-μm-thick anode substrate is one order of magnitude thicker than the 15-μm-thick cathode, concentration polarization is mainly caused by limited gas transport through the thick anode substrate. Although the anode has high porosity (approximately 48 vol.% after reduction), a continuous gas-transport path constituted by larger pores was not thoroughly formed in the anode. It is evident from Fig. 2b that most of pores in the anode are small and closed, and the number of larger pores in the anode is not great enough to allow rapid transport of gases across the anode, resulting in concentration polarization at a high current density.

SDC nanoparticles were formed in the LSM frame using the impregnation method. The major issue for these active SDC nanoparticles in electrodes is their stability during long-term operation at a high temperature (~800 °C). It is evident from Fig. 4 that the voltage of a cell with a 15-μm-thick 3YSZ film at 800 °C decreased with time at a current density of 1.5 A cm^{-2}. This decrease in voltage is caused by coarsening of SDC nanoparticles, which would decrease the ionic conductivity and TPB of the cathode, leading to lower cathode performance and thus lower cell performance. However, the voltage of a cell with a 25-μm-thick 3YSZ film at 700 °C was stable at a current density of 0.5 A cm^{-2}, as shown in Fig. 4. It can be concluded that it is possible to obtain stable cathode performance at 700 °C when the LSM/SDC cathode is sintered at >850 °C, or at 800 °C when the cathode is sintered at a temperature >950 °C.

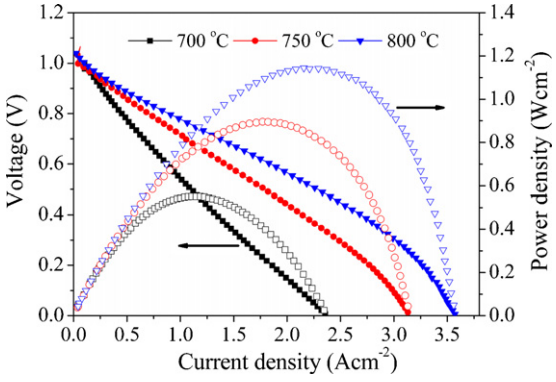

Fig. 3. Electrochemical characteristics of the single cell.

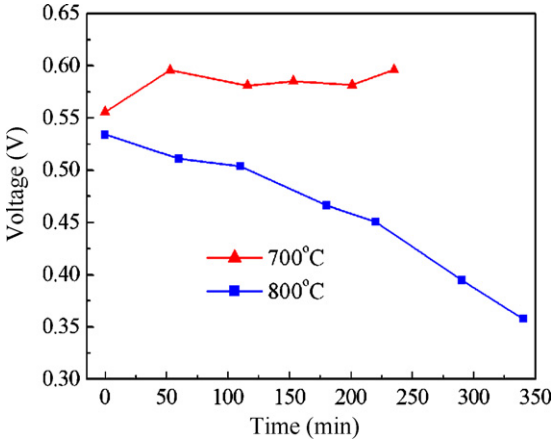

Fig. 4. Voltage–time curve at a current density of 1.5 A cm^{-2} at 800 °C; voltage–time curve at a current density of 0.5 A cm^{-2} at 700 °C.

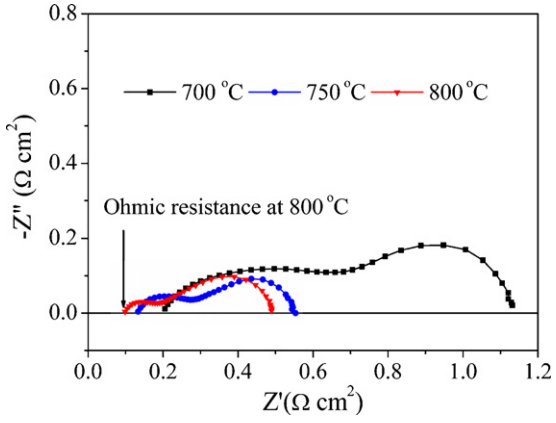

Fig. 5. Impedance spectra of the cell tested under open-circuit conditions.

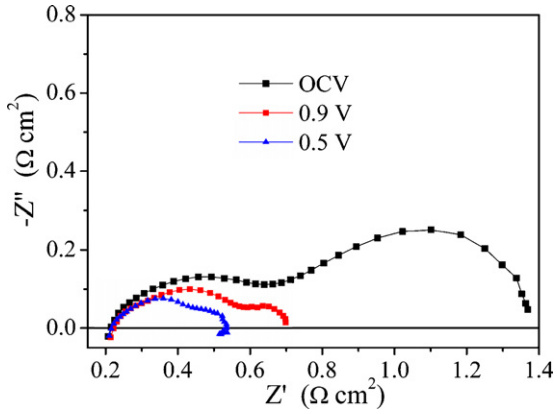

Fig. 6. Impedance spectra of the cell with a 10-μm-thick 3YSZ film tested at different cell voltages at 750 °C using hydrogen at 200 ml min^{-1} as fuel and stationary air as oxidant.

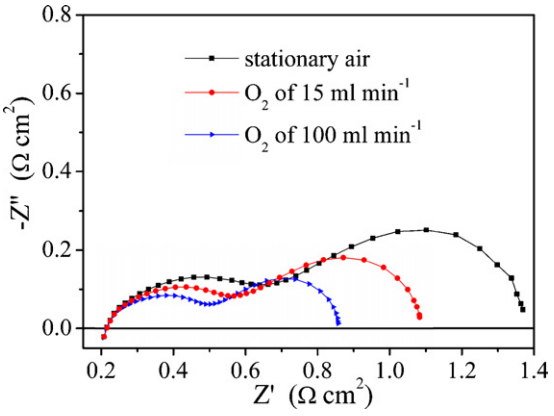

Fig. 7. Impedance spectra of the cell with a 10-μm-thick 3YSZ film tested with oxygen at different flow rates introduced to the cathode at 750 °C.

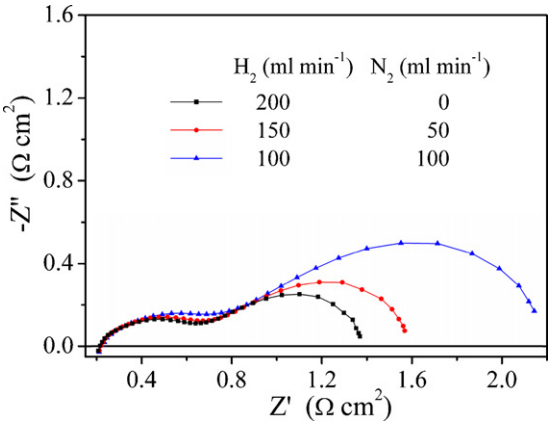

Fig. 8. Impedance spectra of the cell with a 10-μm-thick 3YSZ film tested with fuel gases of different compositions at 750 °C.

It is evident from Fig. 5 that the high-frequency intercept on the real axis represents the ohmic resistance (at 800 °C, for example), which is mainly related to the electrolyte. The difference between the high- and low-frequency intercepts on the real axis shows the electrode polarization resistance of both the anode and cathode. The result shown in Fig. 5 indicates that the electrode polarization resistance dominated the total polarization resistance of the cell at very low current density.

As shown in Fig. 6, both arcs of the impedance spectra decreased with decreasing cell voltage; in particular, the low-frequency arc significantly decreased, indicating decreased electrode polarization resistance, whereas the ohmic resistance remained unchanged. Although the contribution of ohmic resistance to the total cell resistance increased with decreasing cell voltage, the cell performance was still limited by the overwhelming polarization resistance of the electrode, e.g., the electrode polarization resistance accounted for 59% of the total resistance at a cell voltage of 0.5 V, at which the maximum power density often occurred. This reveals that 3YSZ film can be used for fabrication of SOFCs even though its ionic conductivity is not as high as that of 8YSZ.

The high-frequency arc is due to transfer of oxygen ions and the low-frequency arc is due to dissociative adsorption and/or surface diffusion [24]. Since electrochemical oxidation of hydrogen at the anode is much faster than reduction reaction of oxygen at the cathode, activation polarization of the anode is negligible compared to that of the cathode. Therefore, the high-frequency arc—which was not affected by a change in hydrogen partial pressure at the anode, as shown in Fig. 8, but decreased with increasing oxygen partial pressure at the cathode—was caused by the activation polarization resistance of the cathode. The low-frequency arc was then affected by the concentration polarization resistances of both the anode and cathode, as shown in Figs. 7 and 8. The concentration polarization resistance of the electrode with oxygen at 100 ml min^{-1} was half that of the electrode with stationary air, as shown in Fig. 7. This decrease in polarization resistance of the electrode was attributed to the improvement in cathode performance. Thus, it can be concluded that the polarization resistance of the cathode for the low-frequency arc, i.e., the decrease in polarization resistance of the cathode plus the remaining polarization resistance of the cathode, dominates the concentration polarization resistance of the electrode under open-circuit conditions. As shown in Fig. 6, the polarization resistance of the electrode associated with the low-frequency arc largely decreased with decreasing cell voltage. The activation polarization resistance of the cathode associated with the high-frequency arc thus dominated the total polarization resistance of the electrode at the voltage at which maximum power density occurred. As shown in Fig. 8, the low-frequency arc increased dramatically with decreasing hydrogen partial pressure, demonstrating that the gas-transport resistance of the anode was sensitive to the hydrogen partial pressure. At a high current density, the hydrogen partial pressure in the inner anode layer adjacent to the 3YSZ film would decrease rapidly, causing a rapid increase in the concentration polarization resistance of the anode. This is supported by the negative curvature of the *I–V* curves at high current density, as shown in Fig. 3. In summary, it can be concluded that the cell performance was dominated by the polarization of the cathode at lower current densities and was then dominated by the concentration polarization of the anode at higher current densities.

We successfully fabricated a dense 3YSZ electrolyte film by slurry spin coating. The acceptable output performance obtained for single cells indicates that 3YSZ is a potential electrolyte for fabrication of SOFCs. Other methods such as tape casting [6,7] could be used to fabricate dense 3YSZ films for scale-up production.

4. Conclusions

A dense and uniform 3YSZ electrolyte thin film of 6 μm in thickness was fabricated using slurry spin coating on a porous NiO/3YSZ anode substrate. An OCV of 1.04 V was achieved at 800 °C, and maximum power density of 551, 895 and 1143 mW cm^{-2} at 700, 750 and 800 °C, respectively. Impedance spectra results indicated that the cell performance was determined by the polarization resistance of the cathode.

Acknowledgement

The authors thank the Ministry of Science and Technology of China for its financial support under Contract No. 2007AA05Z139.

References

[1] L. Zhang, S.P. Jiang, W. Wang, Y.J. Zhang, J. Power Sources 170 (2007) 55–60.
[2] Q.S. Zhu, B.A. Fan, Solid State Ionics 176 (2005) 889–894.
[3] P. Charpentier, P. Fragnaud, D.M. Schleich, E. Gehain, Solid State Ionics 135 (2000) 373–380.
[4] J. Kim, Y.S. Lin, J. Membr. Sci. 139 (1998) 75–83.
[5] Y.Y. Chen, W.C.J. Wei, Solid State Ionics 177 (2006) 351–357.
[6] J.H. Song, S.I. Park, J.H. Lee, H.S. Kim, J. Mater. Process. Technol. 198 (2008) 414–418.
[7] H. Moon, S.D. Kim, S.H. Hyun, H.S. Kim, J. Hydrogen Energy 33 (2008) 1758–1768.
[8] X.D. Ge, X.Q. Huang, Y.H. Zhang, Z. Lu, J.H. Xu, K.F. Chen, D.W. Dong, Z.G. Liu, J.P. Miao, W.H. Su, J. Power Sources 159 (2006) 1048–1050.
[9] P. Lenormand, D. Caravaca, C. Laberty-Robert, F. Ansart, J. Eur. Ceram. Soc. 25 (2005) 2643–2646.
[10] K.F. Chen, Z. Lü, N. Ai, X.Q. Huang, Y.H. Zhang, X.S. Xin, R.B. Zhu, W.H. Su, J. Power Sources 160 (2006) 436–438.
[11] N. Ai, Z. Lü, K.F. Chen, X.Q. Huang, Y.W. Liu, R.F. Wang, W.H. Su, J. Membr. Sci. 286 (2006) 255–259.
[12] R. Hui, Z.W. Wang, S. Yick, R. Maric, D. Ghosh, J. Power Sources 172 (2007) 840–844.
[13] J.M. Wang, Z. Lu, K.F. Chen, X.Q. Huang, N. Ai, J.Y. Hu, Y.H. Zhang, W.H. Su, J. Power Sources 164 (2007) 17–23.
[14] Z.X. Lu, Y.W. Yu, R.S. Guo, H.L. Li, Q. Guo, Rare Met. 25 (2006) 378–383.
[15] S. Tekeli, Mater. Lett. 57 (2002) 715–719.
[16] S. Jou, T.W. Chi, Vacuum 81 (2007) 911–919.
[17] H. Conrad, D. Yang, Acta Mater. 55 (2007) 6789–6797.
[18] J. Chevalier, S. Deville, E. Munch, R. Jullian, F. Lair, Biomaterials 25 (2004) 5539–5545.
[19] K.F. Chen, Z. Lü, X.J. Chen, N. Ai, X.Q. Huang, B. Wei, J.Y. Hu, W.H. Su, J. Alloys Compd. 454 (2008) 447–453.
[20] W.T. Bao, Q. Chang, G.Y. Meng, J. Membr. Sci. 259 (2005) 103–109.
[21] P.V. Dollen, S. Barnett, J. Am. Ceram. Soc. 88 (2005) 3361–3368.
[22] K.F. Chen, Z. Lü, N. Ai, X.J. Chen, X.Q. Huang, W.H. Su, J. Power Sources 180 (2008) 301–308.
[23] J.Y. Hu, Z. Lü, K.F. Chen, X.Q. Huang, N. Ai, J.M. Wang, W.H. Su, J. Membr. Sci. 318 (2008) 445–451.
[24] Y.J. Leng, S.H. Chan, K.A. Khor, S.P. Jiang, Int. J. Hydrogen Energy 29 (2004) 1025–1033.